in our previous papers in this series.[20]

Acknowledgment. We express our thanks to Professor Yoichi Shimura of Osaka University for making the CD and MCD spectra available. We also wish to thank Dr. Kan Kanamori of Toyama University for obtaining the IR spectra in D_2O and Professor Hiroshi Ogino of Tohoku University for his kind supply of the (*S*)-pdta complex, which facilitated undertaking an initial stage of this research.

(20) Kaizaki, S.; Ito, M.; Nishimura, N.; Matsushita, Y. *Inorg. Chem.* **1985**, *24*, 2080 and references therein.

Registry No. Na[Cr{(*S*)-pdta}], 102734-05-4; Na[Cr{(*S*,*S*)-cydta}], 102734-06-5; Cr{(*S*,*S*)-cydtra}(H_2O), 102649-33-2; Cr{H(*S*)-pdta}(H_2O), 102734-07-6; Cr{H(*S*,*S*)-cydta}(H_2O), 64470-17-3; K[Cr(edta)], 102682-02-0; Cr(hedtra)(H_2O), 40184-49-4; Cr(Hedta)(H_2O), 76582-41-7; Na[Cr(*rac*-cydta)], 33897-09-5; Cr(edtra)(H_2O), 55622-34-9.

Contribution from the Department of Chemistry and Biochemistry, University of California at Los Angeles, Los Angeles, California 90024

Single-Crystal Polarized Electronic Absorption Spectra and Ligand Field Parameters for Triphenylphosphine and Triphenylarsine in $PtCl_3L^-$ Complexes

Tsu-Hsin Chang and Jeffrey I. Zink*

Received October 18, 1985

The single-crystal polarized electronic absorption spectra of $(Pr_4N)[PtCl_3PPh_3]$ and $(Pr_4N)[PtCl_3AsPh_3]$ taken at 10 K are reported. Spin-allowed and spin-forbidden ligand field transitions and a ligand-localized transition are assigned. The σ and π interactions of the triphenylphosphine and triphenylarsine ligands with the metal d orbitals are obtained by using two methods. First, the trends in the σ and π interactions are determined from trends in the energies of spectral features. Second, full-matrix angular-overlap ligand field theory calculations including spin–orbit coupling are reported and the AOM σ and π parameters are reported. The two-dimensional spectrochemical series is discussed. Triphenylphosphine is a better σ donor and a poorer π acceptor than triphenylarsine. These two ligands are compared to other ligands of interest in organometallic chemistry.

The experimental determination of the individual σ and π components of the interaction of phosphine and arsine ligands with transition metals and the comparisons of these properties with those of other important ligands in organometallic chemistry are rare. Although the σ and π interactions can be determined from transition energies measured from electronic absorption spectra and interpreted by using the angular-overlap theory, such studies are in practice inhibited by three factors. First, the d–d transitions in complexes containing phosphine and arsine ligands are usually high in energy and are obscured by more intense charge-transfer bands. Second, the extinction coefficients are frequently large, thus preventing single-crystal polarized absorption spectra from being obtained and definitive assignments from being made. Finally, in complexes where the above limitations can be overcome (e.g. tetrahedral cobalt(II) and nickel(II) triphenylphosphine complexes), detailed and definitive information about triphenylphospine was obtained but could not be compared with properties of other ligands of organometallic interest because of the limited number of complexes that can be prepared.

The most detailed information determined by electronic absorption spectroscopy about the σ and π properties of triphenylphosphine has been obtained by Gerloch et al. from tetrahedral Co(II) and Ni(II) complexes.[1-5] Triphenylphosphine was found to be a good σ donor (stronger than halides but slightly poorer than a tertiary amine) and a good π acceptor (stronger than quinoline and halides). Very little is known about the properties of arsine ligands. Studies of das (bis[*o*-phenylenebis(dimethylarsine)]) have shown that its *Dq* values in Fe(II) and Cr(III) complexes are similar to those for ethylenediamine.[6] The σ and π properties, obtained from a series of halide complexes of the form $Fe(das)_2XY^+$, showed that das is a slightly better σ donor than ethylenediamine and a better π acceptor than halides.[7]

A series of compounds that is proving to be amenable to detailed study of the σ and π interactions of ligands of organometallic importance is the $PtCl_3L^{n-}$ series where L can range from "Werner" ligands such as amines, halides, and pseudohalides to ligands of organometallic interest such as olefins, carbenes, CO, phosphines, and arsines.[8-17] The problem of large extinction coefficients has been overcome by using new microspectroscopic techniques that allow polarized electronic spectra of crystals to be obtained even when $\epsilon > 10^3$ mol^{-1} L cm^{-1}.[15,18] Because only the ligand L changes in the series, systematic changes in the σ and π properties of the ligand are accurately measured and interpreted.

We report here spectroscopic results for $[PtCl_3PPh_3]^-$ and $[PtCl_3AsPh_3]^-$. The single-crystal polarized electronic absorption spectra at 10 K, the assignments of the bands, and the angular-overlap σ and π parameters are reported. The σ and π interactions of the ligands with the metal are determined by using two methods. First, the relative trends in the σ interactions, the π interactions, and the covalency (nephelauxetic effect) are determined directly from the trends in the energies of the spectroscopic features. Second, the complete AOM matrix calculation including spin–orbit coupling is reported and the positions of the ligands in the two-dimensional spectrochemical series are discussed.

(1) Gerloch, M.; Hanton, L. R. *Inorg. Chem.* **1981**, *20*, 1046.
(2) Gerloch, M.; Manning, M. R. *Inorg. Chem.* **1981**, *20*, 1051.
(3) Gerloch, M.; Hanton, L. R. *Inorg. Chem.* **1980**, *19*, 1692.
(4) Davies, J. E.; Gerloch, M.; Phillips, D. J. *J. Chem. Soc., Dalton Trans.* **1979**, 1836.
(5) Bertini, I.; Gatteschi, D.; Mani, F. *Inorg. Chem.* **1972**, *11*, 2464.
(6) Feltham, R. D.; Silverthorne, W. *Inorg. Chem.* **1968**, *7*, 1154.
(7) Zink, J. I.; Liu, P.-H.; Anfield, B. *Inorg. Chem.* **1979**, *18*, 1013.
(8) Fenske, R. F.; Martin, D. S.; Ruedenberg, K. *Inorg. Chem.* **1962**, *1*, 441.
(9) (a) Kroening, R. F.; Rush, R. M.; Martin, D. S.; Clardy, J. C. *Inorg. Chem.* **1974**, *13*, 1366. (b) Martin, D. S.; Tucker, M. A.; Kassman, A. J. *Inorg. Chem.* **1965**, *4*, 1682.
(10) Fanwick, P. E.; Martin, D. S. *Inorg. Chem.* **1973**, *12*, 24.
(11) Martin, D. S. *Inorg. Chim. Acta, Rev.* **1971**, *5*, 107.
(12) Patterson, H. H.; Godfrey, J. J.; Khan, S. M. *Inorg. Chem.* **1972**, *11*, 2872.
(13) Francke, E.; Moncuit, C. *Theor. Chim. Acta* **1973**, *29*, 319.
(14) Tuszynski, W.; Gliemann, G., *Z. Naturforsch., A: Phys., Phys. Chim. Kosmophys.* **1979**, *34A*, 211.
(15) Chang, T.-H.; Zink, J. I. *J. Am. Chem. Soc.* **1984**, *106*, 287.
(16) Chang, T.-H.; Zink, J. I. *Inorg. Chem.* **1985**, *24*, 4499.
(17) Phillips, J. R.; Zink, J. I. *Inorg. Chem.* **1986**, *25*, 1503.
(18) Chang, T.-H.; Zink, J. I. *Inorg. Chem.* **1985**, *24*, 4016.

0020-1669/86/1325-2736$01.50/0

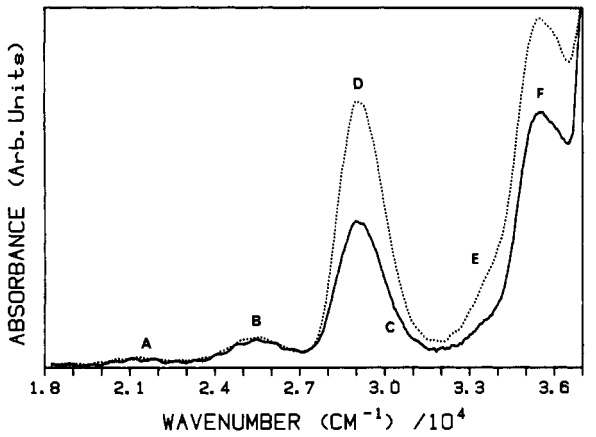

Figure 1. Single-crystal polarized electronic absorption spectrum of $(Pr_4N)[PtCl_3AsPh_3]$ at 10 K: solid line, perpendicular polarization; dotted line, parallel polarization.

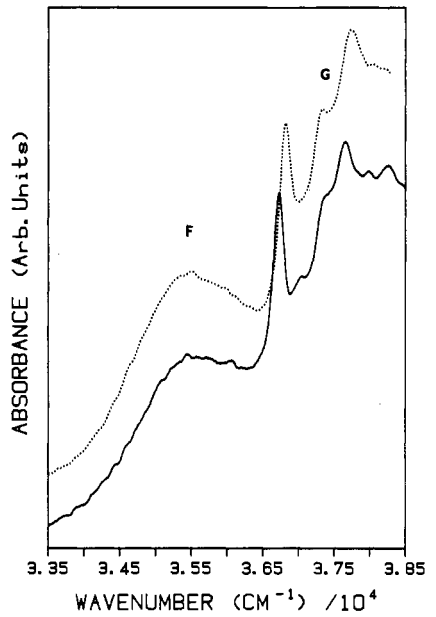

Figure 2. Polarized electronic absorption spectra of an ultrathin single crystal of $(Pr_4N)[PtCl_3AsPh_3]$ at 10 K: solid line, perpendicular polarization; dotted line, parallel polarization.

Experimental Section

The compounds $(Pr_4N)[PtCl_3L]$ (L = PPh_3, $AsPh_3$) were prepared by reacting Pr_4NCl with $Pt_2Cl_4L_2$. The dimer $Pt_2Cl_4L_2$ was prepared by following the procedure of Goodfellow et al.[19,20] A 2:1 mole ratio mixture of Pr_4NCl and $Pt_2Cl_4L_2$ was stirred in CH_2Cl_2 until no solid remained. After filtration, diethyl ether was slowly added. Platelike crystals formed immediately with yields greater than 90%. The products were recrystallized from CH_2Cl_2 and diethyl ether.

The single crystals for spectroscopic measurements of both $(Pr_4N)[PtCl_3PPh_3]$ and $(Pr_4N)[PtCl_3AsPh_3]$ were grown between quartz plates from a dichloromethane solution. A drop of the solution was placed on one plate and a second plate pressed over the first. The plates were stored in the dark. After several hours, crystals having dimensions on the order of 100 × 100 × 0.1 μm were obtained. The crystals of the triphenylphosphine complex were almost square. The spectra were obtained from crystal faces that have the extinction axis about 46° from one of the crystal axes. The crystals of the triphenylarsine complex were rectangular. The spectrum labeled parallel was obtained with the electric vector of the incident radiation parallel to the extinction axis at an angle of 46° to the long crystal axis. The spectrum labeled perpendicular was obtained in the orthogonal extinction direction. The terms perpendicular and parallel are not related to the molecular axes and are only used to differentiate between the orthogonal extinction directions.

(19) Goodfellow, R. J.; Venanzi, L. M. *J. Chem. Soc.* **1965**, 7533.
(20) Goodfellow, R. J.; Goggin, P. L.; Venanzi, L. M. *J. Chem. Soc. A* **1967**, 1892.

Table I. Peak Maxima and Assignments for $(Pr_4N)[PtCl_3AsPh_3]$

abs max, cm^{-1}	assignt	label in Figures 1 and 2
21 260 (20 890)[a]	triplet[b]	A
25 430 (24 620)	triplet[b]	B
29 090 (28 640)	$^1B_1$ $d_{xy} - d_{x^2-y^2}$	D
30 500 (30 000)	triplet[b]	C
33 460 (32 700)	$^1A_2$ $d_{yz} - d_{x^2-y^2}$	E
35 500 (...)	$^1B_2$ $d_{xz} - d_{x^2-y^2}$	F
>37 500[c,d]	π to π^* transition in phenyl ring	G

[a] Values in parentheses are the peak maxima in the room-temperature single-crystal polarized electronic absorption spectrum. [b] The observed bands are caused by clusters of spin–orbit components. [c] The position of this band in the room-temperature spectrum is obscured by the ligand-localized band. [d] Individual vibronic components are resolved, but the position of the band maximum is uncertain.

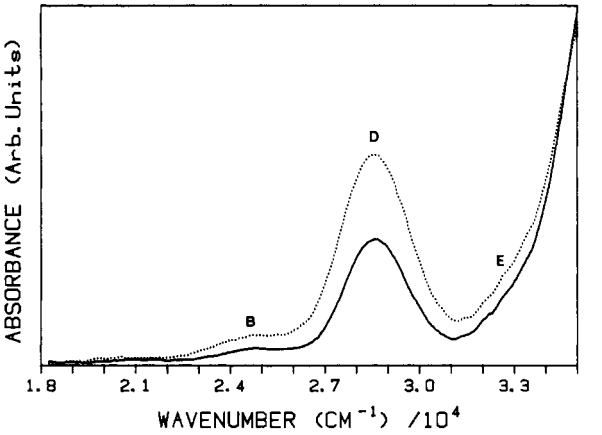

Figure 3. Room-temperature single-crystal polarized electronic absorption spectra of $(Pr_4N)[PtCl_3AsPh_3]$: solid line, perpendicular polarization; dotted line, parallel polarization.

The instrument that was used to obtain the crystal spectra is a locally constructed microspectrophotometer, which has been described previously.[15] The solution-phase spectra were recorded by using a Cary 14 spectrophotometer.

Results

The electronic absorption spectra at 10 K of single crystals of $(Pr_4N)[PtCl_3AsPh_3]$ are shown in Figures 1 and 2. The crystals were rectangular. The parallel spectrum was obtained with the electronic vector of the incident polarized radiation parallel to the extinction axis at an angle of 46.2° to the long crystal axis. The perpendicular spectrum was obtained in the orthogonal extinction direction. Because the crystal structure is not known, the projection of the electric vector of the incident radiation on the molecular axes cannot be determined. The observed polarization changes provide a very useful method for resolving closely spaced features. The spectra in Figure 2 were obtained from ultrathin crystals. The energies of the peaks and shoulders are given in Table I and are labeled as shown in Figures 1 and 2.

The three low-intensity features, labeled bands A through C, are observed in the spectra of the thicker crystals. Band A at 21 260 cm^{-1} and band B at 25 430 cm^{-1} have nonzero intensities in both polarizations. Band C, a shoulder at about 30 500 cm^{-1} on the high-energy side of the more intense band D, is most readily observed in perpendicular polarization.

Bands D and F, at 29 090 and 35 500 cm^{-1}, respectively, are the two most prominent medium-intensity bands. Both are most intense in parallel polarization and are observed in both polarizations. The behavior of these two bands is very similar to that of the analogous bands in $[PtCl_3NMe_3]^-$. Band E at 33 460 cm^{-1} is a shoulder that, unlike its counterpart in the trimethylamine complex, appears to the low-energy side of band F. It is observed in both polarizations but is more intense in parallel polarization. It exhibits a large temperature dependence (vide infra).

At energies above 36 500 cm^{-1} a complicated series of features on an intense band are observed on-scale in the spectra of the

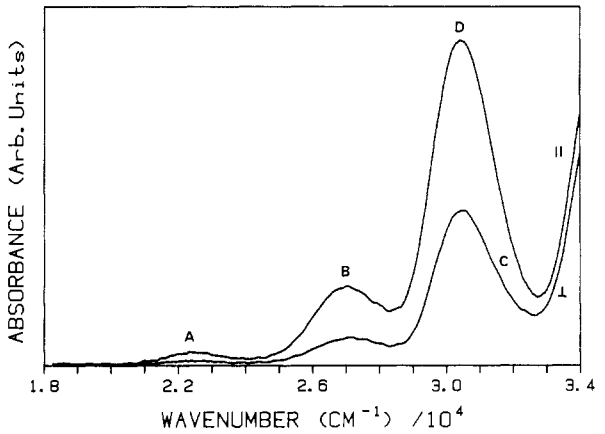

Figure 4. Single-crystal polarized absorption spectra of $(Pr_4N)[PtCl_3PPh_3]$ at 10 K.

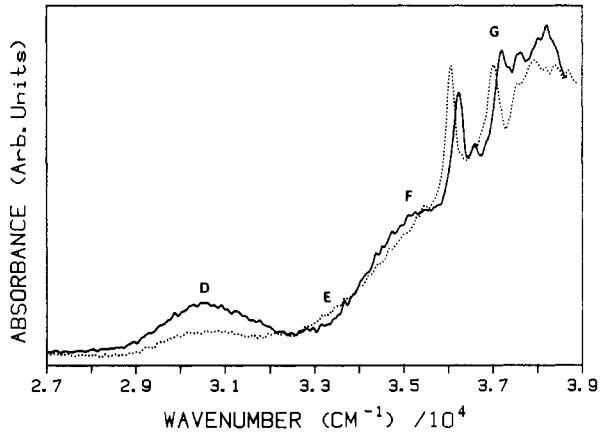

Figure 5. Polarized electronic absorption spectra of an ultrathin crystal of $(Pr_4N)[PtCl_3PPh_3]$ at 10 K: solid line, parallel polarization; dotted line, perpendicular polarization.

ultrathin crystals (Figure 2). These features, which are vibronic components, are collectively labeled G in Figure 2 and Table I.

The room-temperature spectra are shown in Figure 3. Red-shifts and increases in the bandwidths are observed as the temperature is raised. These trends were also observed for the $[PtCl_3L]^-$ compounds previously studied in our laboratory. The positions of the bands are given in Table I. The largest intensity increase was observed for band E. The ratios of the intensities of bands E and D in parallel polarization are roughly 1:2 at room temperature anid roughly 1:4 at low temperature. The corresponding ratios in perpendicular polarization are roughly 1:1.5 and 1:3, respectively.

The 10 K polarized absorption spectra of a thin and an ultrathin single crystal of $(Pr_4N)[PtCl_3PPh_3]$ are shown in Figures 4 and 5, respectively. The spectra were obtained from an almost square crystal face that has one extinction axis 46° from one of the crystal axes.

The spectra of $[PtCl_3PPh_3]^-$ are very similar to those of $[PtCl_3AsPh_3]^-$. The energies of the observed bands are listed in Table II. The bands are labeled the same as those in the analogous arsine complex. The major difference between the spectra of the two compounds is a shift to lower energy of the features constituting band G. This shift causes band G to overlap band F in the PPh_3 complex. The latter band thus appears as a shoulder on the more intense band G (Figure 5). The remaining spectral features, including those in the spectra of the thicker crystals and at room temperature, are so similar to the features in the arsine complex described above that they will not be described further.

The *pattern* of the spectra of $[PtCl_3PPh_3]^-$ and $[PtCl_3AsPh_3]^-$ is very similar to the pattern of the spectra of all of the $PtCl_3L$ complexes that have been studied in our laboratory to date. This pattern consists of two or three low-intensity ($\epsilon < 100$) bands at the low-energy end of the spectrum, three medium-intensity ($\epsilon > 100$), medium-energy bands, one of which is very temperature-dependent, and finally high-intensity features ($\epsilon > 10^3$) at the high-energy side of the spectrum. The energies of the bands of course vary as the ligand L is varied, but the similarity of the pattern simplifies the task of assigning the bands.

Table II. Peak Maxima and Assignments for $(Pr_4N)[PtCl_3PPh_3]$

abs max, cm^{-1}	assignt	label in Figures 3 and 4
22 300 (21 800)[a]	triplet[b]	A
27 040 (26 300)	triplet[b]	B
30 460 (30 000)	$^1B_1$ $d_{xy} - d_{x^2-y^2}$	D
31 500 (31 100)	triplet[b]	C
33 400 (...)	$^1A_2$ $d_{yz} - d_{x^2-y^2}$	E
35 310 (34 800)	$^1B_2$ $d_{xz} - d_{x^2-y^2}$	F
>37 500[c,d]	π to π^* transition in phenyl ring	G

[a] Values in parentheses are the peak maxima in the room-temperature single-crystal polarized electronic absorption spectrum [b] The observed bands are caused by clusters of spin–orbit components. [c] The position of this band in the room-temperature spectrum is obscured by the ligand-localized band. [d] Individual vibronic components are resolved, but the position of the band maximum is uncertain.

Discussion

1. Assignments. The spectra of both $(Pr_4N)[PtCl_3PPh_3]$ and $(Pr_4N)[PtCl_3AsPh_3]$ can be readily assigned from the band patterns in the single-crystal low-temperature polarized spectra, the band intensities, and the temperature dependence of the bands. By comparison of the observed pattern with the very similar patterns from other $PtCl_3L^-$ complexes for which assignments have been made, initial assignments of bands A through F are made. The relative polarizations support the assignments. The extinction coefficients provide further confirmation of the singlet and triplet assignments. The temperature dependences, including both intensity and energy changes, provide additional confirmation. All of these aspects of the assignments are discussed below. In the discussion, the $[PtCl_3L]^-$ ions are treated in the C_{2v} point group with the z axis perpendicular to the square plane and the x axis along the Pt–L bond. The assignments are given in Tables I and II.

In both the PPh_3 and $AsPh_3$ complexes, the three low-energy, low-intensity bands, bands A through C, are assigned to spin-forbidden transitions. These bands are comprised of clusters of spin–orbit coupled components from the $^3A_2$, $^3B_1$, and $^3A_1$ states. The spacings, relative polarizations, and relative intensites are very similar to those of the three triplet bands in the NMe_3 complex.[16] The details of the spin–orbit states are discussed in the following section.

The two prominent bands at higher energy and higher intensity, bands D and F, are assigned to the spin-allowed d–d transitions $^1A_1 \rightarrow {}^1B_1$ and $^1A_1 \rightarrow {}^1B_2$, $d_{xy} \rightarrow d_{x^2-y^2}$ and $d_{xz} \rightarrow d_{x^2-y^2}$, respectively. Band D, which is resolved in the solution spectra of both the $[PtCl_3PPh_3]^-$ and $[PtCl_3AsPh_3]^-$ compounds, has an extinction coefficient of $\epsilon = 410$ and 375 L mol^{-1} cm^{-1}, respectively. These values are the usual magnitudes of singlet d–d transitions for square-planar Pt(II) complexes.

The shoulder to the low-energy side of band F in the low-temperature spectra, labeled band E, is the dipole-forbidden singlet d–d transition $^1A_1 \rightarrow {}^1A_2$, $d_{yz} \rightarrow d_{x^2-y^2}$. Pattern recognition is not useful in helping to assign this band because its position in the spectrum of $[PtCl_3L]^-$ complexes is the most variable (vide infra). However, its intensity is temperature-dependent. This behavior is expected for a vibronically allowed, dipole-forbidden transition and is also observed for the $^1A_2$ band in all of the $[PtCl_3L]^-$ compounds.

The roughly twofold increase in the intensity as the temperatue is raised from 10 to 300 K supports the assignment to the vibronically allowed $^1A_2$ band. The severe overlapping of the bands prevents detailed calculations from being made. On the assumption that the intensity of band D is temperature independent, the intensity of band E is calculated to increase by a factor of 2. A crude calculation shows that the expected increase, which should

exhibit a coth ($h\nu/2kT$) temperature dependence,[21] requires a vibrational energy of about $h\nu$ = 240 cm^{-1}. Platinum–chloride modes of the proper symmetries occur around 290–310 cm^{-1}.[22,23] Thus the magnitude of the temperature increase supports the assignment.

The collection of sharp features, collectively labeled band G in Figures 2 and 5, are assigned to a π–π^* intraligand transition. The corresponding band in the solution spectrum of $[PtCl_3PPh_3]^-$ occurs at 37 800 cm^{-1} with ϵ = 2300 L mol^{-1} cm^{-1}. In the spectrum of $[PtCl_3AsPh_3]^-$ the band occurs at 37 600 cm^{-1} with ϵ = 6700 L mol^{-1} cm^{-1}. The large extinction coefficients preclude an assignment to a d–d transition. The lowest energy sharp band in the crystal spectra at low temperature are at 36 040 cm^{-1} in the PPh_3 complex and at 36 730 cm^{-1} in the $AsPh_3$ complex. The similarity of the transition energies suggests that the transition involves orbitals primarily localized on the phenyl rings and rules out a charge-transfer or ligand-localized transition that primarily involves orbitals on the phosphorus or arsenic atoms. The exact position of the band maximum cannot be determined from the crystal spectrum because the band is located at the lower wavelength limit accessible in this experiment.

2. Calculations of the Transition Energies and the Ligand Field Parameters. The transition energies are treated by the angular-overlap model (AOM) in terms of parameters representing the σ and π interactions between the metal and the ligands. For example, the energy of the $d_{x^2-y^2}$ orbital will depend on its σ interactions with the chloride ligands, e_σ^{Cl}, and the σ interaction with the phosphine or arsine, e_σ^{P} or e_σ^{As}, respectively. Correspondingly, the d_{xy} orbital energy will depend on the in-plane π interactions with these ligands, e_π^{Cl}, e_π^{P}, or e_π^{As}. The state energies are calculated from the one-electron orbital energies by using the symmetry-adapted wave functions and evaluating the matrix elements. The electron-repulsion energies are expressed in terms of the Racah parameters B and C. The matrix elements have been tabulated and will not be repeated here.[13] Finally, the transition energies are calculated by diagonalizing the complete energy matrix and calculating the energy differences between the ground state and the various excited states.

Two methods of treating the spectra of the $[PtCl_3L]^-$ compounds will be discussed. The most complete method is the full-matrix calculation, including spin–orbit coupling, of the transition energies as a function of the ligand field parameters. The results of this calculation are discussed later. First, only the diagonal elements are examined. Physical insight into the meaning of the transition energies is obtained from this simplified method, but accurate numerical values of the parameters cannot be obtained.

Three quantities that can be obtained directly from the experimental spectrum are important to the interpretation: the energy difference between the lowest singlet and lowest triplet states, eq 1, the energy of the $^1A_2$ transition, eq 2, and the energy difference between the $^1B_2$ and the $^1A_2$ states, eq 3.

$$\Delta E(^1B_1) - \Delta E(^3B_1) = 2C \quad (1)$$

$$\Delta E(^1A_2) = -3B - C + \tfrac{3}{4}(3e_\sigma^X + e_\sigma^L) - 2e_\pi^X \quad (2)$$

$$\Delta E(^1B_2) - \Delta E(^1A_2) = e_\pi^X - e_\pi^L \quad (3)$$

The trend in the nephelauxetic series can be estimated from the trend in the singlet–triplet energy spacing in the spectra. This spacing is equal to $2C$ for the singlet and triplet B_1 states. (For other states, both B and C are involved.) The smaller the value of C, the smaller the electron repulsion energy and the larger the covalency. The experimentally determined trend is given in Table III. The nephelauxetic series in order of increasing covalency is thus $Cl \cong PEt_3 < NMe_3 < PPh_3 < AsPh_3 < C_2H_4$.

Table III. Trends in Experimentally Measured Energies

unique ligand	singlet–triplet energy diff, cm^{-1}	$^1A_2$ energy, cm^{-1}	$^1B_2$–$^1A_2$ energy diff, cm^{-1}
PEt_3[a]	8700[f]	36 200	−500
NMe_3[b]	8330	34 850	−2140
PPh_3[c]	8160	33 400	1910
$AsPh_3$[c]	7830	33 458	2040
C_2H_4[d]	7390	30 350	2450
Cl^-[e]	8700	29 200	0

[a] Reference 17. [b] Reference 16. [c] This work. [d] Reference 15. [e] References 13 and 24. [f] Energy difference between the lowest observed singlet and triplet absorption bands.

Table IV. Calculated and Observed Transition Energies (cm^{-1}) for $[PtCl_3PPh_3]^-$

calcd[a]	obsd	assignt	label
	Singlets		
30 450	30 460	$^1B_1$	D
33 199	33 400	$^1A_2$	E
35 211	35 310	$^1B_2$	F
38 113	*b*	$^1A_1$	...
	Triplets		
20 237		A_1	
20 264	21 000[c]	B_2	
20 458		B_1	
21 953		A_2	
22 553	22 300	B_1	A
23 884		A_1	
24 092		A_2	
24 115		B_2	
26 453		A_1	
26 857	27 040	B_2	B
27 203		A_2	
29 231		B_1	
	31 500		C

[a] The transition energies were calculated by using the following parameters (cm^{-1}): e_σ^{Cl} = 11 800, $e_{\pi,\parallel}^{Cl}$ = 2770, $e_{\pi,\perp}^{Cl}$ = 3180, e_σ^{P} = 20 000, $e_{\pi,\parallel}^{P}$ = 2400, $e_{\pi,\perp}^{P}$ = 620; B = 1520, C = 2900, e_{sd} = 15 900, ξ = 2900. The π parameters have in-plane ($\parallel$) and out-of-plane ($\perp$) components. The mean value is discussed in the text. [b] Obscured by the π–π^* transition. The calculated energy includes s–d mixing. [c] Broad, ill-defined shoulder.

The trend in the σ-donor ability of the ligand L can be estimated from the trend in the energy of the $^1A_2$ state. The trend in this energy, given in eq 2, is dominated by the trend of e_σ^L because the energy contribution from the Racah parameters only varies by several 10^2 cm^{-1} from compound to compound, and the parameters from the chloride ligand are roughly constant from compound to compound in the $PtCl_3L^{n-}$ series (vide infra). The $^1A_2$ transition energies are listed in Table III. The trend in the σ-donor ability of the ligands increases in the order $Cl < C_2H_4 < AsPh_3 < PPh_3 < NMe_3$.

The trend in the π interactions between the ligand L and platinum can be estimated from the trend in the $^1B_2$–$^1A_2$ energy separation in the experimental spectra. This energy difference, according to eq 3, varies with e_π^L as the ligand L is changed. The contribution from e_π^{Cl} is roughly constant from compound to compound. The experimentally determined energy separation is given in Table III. Because this estimate does not take into account the parallel and perpendicular components, the detailed order is uncertain and the π-donor trend is conservatively determined to be $NMe_3 > (PEt_3, Cl^-) > (PPh_3, AsPh_3, C_2H_4)$.

AOM Energy Matrix Calculations

The singlet and triplet transition energies for the phosphine and arsine complexes calculated by diagonalizing the AOM energy matrix are given in Tables IV and V, respectively. The AOM parameters that were used are included in the tables. The same assumptions as those discussed and used in previous work were employed in these calculations; i.e., the chloride parameters and the spin–orbit coupling constant were assumed to be transferable

(21) Ballhausen, C. J. *Introduction to Ligand Field Theory*; McGraw-Hill: New York, 1962; p 187.
(22) Adams, D. M. *Metal-Ligand and Related vibrations*; *arnold*: London, 1967.
(23) Poulet, H.; Delorme, P.; Mathieu, J. P. *Spectrochim. Acta* **1964**, *20*, 1855.

Table V. Calculated and Observed Transition Energies (cm^{-1}) for $[PtCl_3AsPh_3]^-$

calcd[a]	obsd	assignt	label
	Singlets		
30 638	29 090	$^1B_1$	D
33 465	33 460	$^1A_2$	E
35 506	35 500	$^1B_2$	F
37 661	*b*	$^1A_1$	...
	Triplets		
21 055		A_1	
21 196		B_2	
21 752	21 260	B_1	A
22 310		A_2	
23 947		B_1	
23 975	25 430	B_2	B
24 677		A_2	
24 847		A_1	
26 876		A_1	
27 765		B_2	
27 989	30 500	A_2	C
29 105		B_1	

[a] The transition energies were calculated by using the following parameters (cm^{-1}): $e_\sigma^{Cl} = 11\,800$, $e_{\pi,\parallel}^{Cl} = 2740$, $e_{\pi,\perp}^{Cl} = 2870$, $e_\sigma^{As} = 18\,000$, $e_{\pi,\parallel}^{As} = 1900$, $e_{\pi,\perp}^{As} = 300$, $B = 600$, $C = 2760$, $\sigma_{sd} = 14\,900$, $\xi = 2900$. The π parameters have in-plane ($\parallel$) and out-of-plane ($\perp$) components. The mean value is discussed in the text. [b] Obscured by the π–π^* transition. The calculated enregy includes s–d mixing.

within the narrow range of several hundred wavenumbers.

The quantitative agreement between the calculated and observed singlet-state transition energies is very good. The mean discrepancy between the measured and calculated singlet-state transition energies is 314 cm^{-1}. The calculations also are in agreement with the assignments made in the previous section. The position of the $^1A_1$ state is calculated to be under the intense ligand-localized transition.

The calculated transition energies of the triplet states also agree well with the observed transitions. The calculation, including spin–orbit coupling, shows that the observed bands do not arise from a single "triplet" state such as $^3B_1$ but instead are composed of clusters of spin–orbit-coupled components. These results illustrate why polarization properties alone cannot be used to assign these states. The intensities depend strongly on the amount of singlet character that is mixed into each component.

The ligand field parameters that are obtained from the matrix calculation follow the trends expected from the diagonal elements as discussed above. The accuracy of the σ and π parameters is on the order of ± 500 cm^{-1}. This range of uncertainty is based on experience with the transferability of the parameters from one compound to another. In the most careful test of the transferability to date, we used the ethylene and bromide parameters to calculate the spectrum of $[PtBr_3(C_2H_4)]^-$. A very good fit was obtained when the parameters were transferred directly (i.e., the maximum difference between the calculated band positions and those observed in the single-crystal polarized spectrum was less than 1000 cm^{-1}). When the parameters were allowed to vary to obtain the best fit to the spectrum, we found that varying the σ and π parameters within the +500-cm^{-1} range enabled us to obtain an excellent fit (differences less than 200 cm^{-1}).

Two-Dimensional Spectrochemical Series for $[PtCl_3L]^{n-}$

The two-dimensional spectrochemical series for the ligands studied to data is shown in Figure 6. The ligand field σ and π parameters, determined by using the full-energy-matrix calculations, are plotted as a function of their σ-donor and π-donor properties. The uncertainties, indicated by the error bars, are small enough to allow the trends to be clearly discerned. Of the ligands studied to date, ethylene is the best π acceptor and triethylphosphine is the best σ donor. Both PPh_3 and $AsPh_3$ are very good π acceptors, with $AsPh_3$ being slightly better than PPh_3. The phosphine is a significantly better σ donor than the arsine. Chloride is a better π-donor and a better σ-donor ligand than

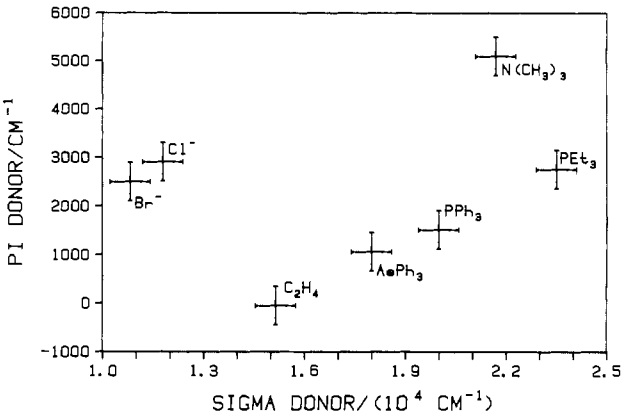

Figure 6. Two-dimensional spectrochemical series for the PtX_3L^{n-} series.

bromide although both of these ligands' π-donor ability is smaller than might have been expected.

The σ-donor parameters determined by the AOM calculation follow the order $PET_3 > NMe_3 > PPh_3 > AsPh_3 > C_2H_4 > Cl > Br$. This series, determined from the $PtCl_3L^-$ complexes studied to date, is still too small to allow sweeping generalization to be made. Note that in this series the σ-donor ability of the trialkylphosphine is greater than that of the triphenylphosphine. Also, the phosphines are better donors than the arsine. Perhaps the only surprise in the above series is the result that the trialkylphosphine is a better σ donor than the trialkylamine. Note also that ethylene is a surprisingly good σ donor; its position in the quantitative σ series is about halfway between that of chloride and triphenylarsine.

The trends in the π-acceptor series are somewhat more difficult to interpret. Consider first only the ligands L in the $[PtCl_3L]^-$ series. For these ligands, the quantitative order of π-acceptor ability is $C_2H_4 > AsPh_3 > PPh_3 > PEt_3 > NMe_3$. This order is generally that expected from the trends obtained from CO stretching frequencies in L-substituted carbonyl complexes. However, the position of the halides, taken at face value, is very surprising. The numerical values place chloride about equal to triethylphosphine in the π series. Furthermore, the e_π^{Cl} value for chloride places it as a poorer π donor (better π acceptor) than trimethylamine. It has long been known that the AOM π parameter for amines is not zero. When a complete fit to experimental spectra is obtained and the π value for amine is allowed to vary in order to obtain the best fit, the π value generally is greater than zero.[24] (Reported values of zero are usually based on the assumption that $e_\pi^N = 0$.) We interpret the large positive π values for ligands with large σ-donor parameters as a manifestation of the electrostatic interactions between the lone pair on the donor atom of the ligand with the metal d orbitals. Thus in the square-planar complexes, both the d_{xy} and the d_{xz} orbitals are raised in energy by the electrostatic interaction. This type of interaction should be particularly evident when the e_σ values are very large as is the case for NMe_3 and PEt_3.[25]

A meaningful interpretation of the trends in the π-interaction properties of ligands can be obtained by considering the value of the AOM π parameter relative to that of the σ parameter, i.e. the value of e_π^L/e_σ^L. This normalized π value takes into account the magnitude of the electrostatic interaction by assuming that it is proportional to the σ interaction of the lone pairs on the ligand with the metal orbitals. A similar interpretation has been introduced to explain the otherwise surprising d-orbital ordering in a series of metal porphyrin complexes.[26] When the ligands in Figure 5 are ordered in terms of the normalized π parameter

(24) Vanquickenborne, L. G.; Ceulemans, A. *Inorg. Chem.* **1981**, *20*, 796.
(25) A similar interpretation has been presented for strong σ-donor ligands in chromium(III) complexes: Keeton, M.; Chou, B. F.; Lever, A. B. P. *Can. J. Chem.* **1971**, *49*, 1971.
(26) Byrn, M. P.; Katz, B. A.; Keder, N. L.; Levan, K. R.; Magurany, C. J.; Miller, K. M.; Pritt, J. W.; Strouse, C. E. *J. Am. Chem. Soc.* **1983**, *105*, 4916.

e_π^L/e_σ^L, the order in terms of decreasing π-acceptor ability is C_2H_4 > $AsPh_3$ > PPh_3 > PEt_3 > NMe_3 > Cl. This order of normalized π-acceptor ability places chloride as a poorer π acceptor than the amine, the position it occupies in the high-oxidation-state "Werner" complexes.

Acknowledgment. The support of this research by the National Science Foundation is gratefully acknowledged.

Registry No. PPh_3, 603-35-0; $AsPh_3$, 603-32-7; $[Pr_4N][PtCl_3PPh_3]$, 19508-39-5; $[Pr_4N][PtCl_3AsPh_3]$, 102493-30-1; $Pt_2Cl_4(PPh_3)_2$, 15349-80-1; $Pt_2Cl_4(AsPh_3)_2$, 39539-17-8.

Contribution from the Laboratoire de Spectrochimie du Solide (LA 302), Université Paris VI, 75230 Paris Cedex 05, France

ESR and ENDOR Study of the Electronic Structure of the Radical Anion $[[CH_3N(PF_2)_2]_3Co_2(CO)_2]^-$

F. Babonneau* and J. Livage

Received November 26, 1985

The ESR spectrum of the radical anion $[[CH_3N(PF_2)_2]_3Co_2(CO)_2]^-$ indicates complete delocalization over the two cobalt sites even at 4 K. The unpaired electron is in the intermetallic σ^* molecular orbital, mainly localized onto the cobalt orbitals: $\rho(Co,d_{z^2})$ = 0.38, and $\rho(Co,4s)$ = 0.006-0.013. The hyperfine couplings with the phosphorus and fluorine nuclei show a little extension of the unpaired electron density on the equatorial fluorophosphine ligands. ENDOR experiments were undertaken: a dipolar coupling between the unpaired electron and the methyl protons is revealed. Other proton signals appeared, which were assigned to one or several protons located on the amino groups. A fluorine ENDOR spectrum was also obtained, which confirmed the hyperfine coupling values first deduced from the ESR spectra. Extended Hückel calculations are presented that are consistent with the description of the ground-state molecular orbital deduced from ESR and ENDOR experiments.

The electronic structure of polynuclear transition-metal complexes is of current interest.[1-6] ESR appears to be a very powerful technique for studying such complexes when they are paramagnetic. Otherwise, in the case of diamagnetic compounds, it is sometimes possible to get a paramagnetic radical ion through redox reactions. ESR then gives indirect information on the HOMO or LUMO of the parent neutral complex.[7-9] However, the metal-metal bond is often so weak that redox reactions lead to the dissociation of the complex. It would be therefore quite interesting to synthesize bridging ligands that are able to stabilize the metal-metal bond toward redox reactions. Stable radical ions can then be obtained and spectroscopic studies easily performed.[10] Dinuclear complexes with bis(difluorophosphino)alkylamino bridging ligands have been recently synthesized from cobalt,[10-12] iron,[13-15] and molybdenum[16] carbonyl compounds. The cobalt dinuclear derivative $[CH_3N(PF_2)_2]_3Co_2(CO)_2$ undergoes a reversible one-electron reduction, giving rise to a radical anion that remains stable under an inert atmosphere.[17]

An ESR study of the paramagnetic $[[CH_3N(PF_2)_2]_3Co_2(CO)_2]^-$ radical anion was recently published.[18] It showed that the unpaired electron was equally delocalized over the two cobalt units in a σ^* metal-metal molecular orbital. The complex then belongs to class III of the mixed-valence compounds, according to the classification suggested by Robin and Day.[19] Some information about electron delocalization over the ligands were obtained from the hyperfine structure of the spectrum. But, due to the line width, some hyperfine couplings were not resolved.

In this paper, we present an ENDOR study giving more details about the different hyperfine interactions together with LCAO-MO calculations of the electronic structure of the complex.

Experimental Results

A. ESR Results. X- and Q-band ESR spectra have already been published.[18] They were analyzed by trial and error comparison with simulated spectra.[20] They show that, even at 4 K, the unpaired electron remains equally delocalized over the two cobalt units.

The following **g** tensor values were determined from both room- and low-temperature spectra assuming an axial symmetry: $g_\perp$ = 2.03; $g_\parallel$ = 2.00; g_0 = 2.025.

The hyperfine structure of the ESR spectra also provided information about the couplings between the unpaired electron and some nuclei having a nonzero nuclear spin. For cobalt, $|A_0(Co)|$ = 18 G, $|A_\perp(Co)|$ = 48 G, and $|A_\parallel(Co)|$ = 38 G; for phosphorus, $|A_0(P)|$ = 42.7 G, $|A_\perp(P)|$ = 42.7 G, and $|A_\parallel(P)|$ = 42.7 G; for fluorine, $|A_0(F)|$ = 5.3 G.

(1) Symons, M. C. R.; Bratt, S. W. *J. Chem. Soc., Dalton Trans.* **1979**, 1739.
(2) Peake, B. M.; Rieger, P. H.; Robinson, B. H.; Simpson, J. *J. Am. Chem. Soc.* **1980**, *102*, 156.
(3) Cotton, F. A.; Pedersen, E. *J. Am. Chem. Soc.* **1975**, *97*, 303.
(4) Kawamura, T.; Fukamachi, K.; Hayashida, S. *J. Chem. Soc., Chem. Commun.* **1979**, 94S.
(5) Strouse, C. E.; Dahl, L. F. *Discuss. Faraday Soc.* **1969**, *47*, 93.
(6) Hayashida, S.; Kawamura, T.; Yanezawa, T. *Inorg. Chem.* **1982**, *21*, 2235.
(7) Cotton, F. A.; Pedersen, E. J. *J. Am. Chem. Soc.* **1975**, *97*, 303.
(8) Bratt, S. W.; Symons, M. C. R. *J. Chem. Soc., Dalton Trans.* **1977**, 1314.
(9) Kawamura, T.; Hayashida, S.; Yonezawa, T. *Chem. Lett.* **1980**, 517.
(10) King, R. B. *Acc. Chem. Res.* **1980**, *13*, 243.
(11) Newton, M. G.; King, R. B.; Chang, M.; Pantaleo, N. S.; Gimeno, J. *J. Chem. Soc., Chem. Commun.* **1977**, 531.
(12) King, R. B.; Gimeno, J.; Lotz, T. J. *Inorg. Chem.* **1978**, *17*, 2401.
(13) King, R. B.; Gimeno, J. *Inorg. Chem.* **1978**, *17*, 2390.
(14) Newton, M. G.; King, R. B.; Chang, M.; Gimeno, J. *J. Am. Chem. Soc.* **1977**, *99*, 2802.
(15) King, R. B.; Lee, T. W.; Kim, J. H. *Inorg. Chem.* **1983**, *22*, 2964.
(16) King, R. B.; Shimura, M.; Brown, G. M. *Inorg. Chem.* **1984**, *23*, 1398.
(17) Chaloyard, A.; El Murr, N.; King, R. B. *J. Organ. Chem.* **1980**, *188*,C 13.
(18) Babonneau, F.; Henry, M.; El Murr, N.; King, R. B. *Inorg. Chem.* **1985**, *24*, 1946.
(19) Robin, M. D.; Day, P. *Adv. Inorg. Chem. Radiochem.* **1967**, *10*, 248.
(20) For analysis of the ESR spectra, a simulation programm REPELEC was used on the basis of a second-order perturbation solution of the spin Hamiltonian.

0020-1669/86/1325-2741$01.50/0